Ceramics International 50 (2024) 53701–53711

Contents lists available at ScienceDirect

Ceramics International

journal homepage: www.elsevier.com/locate/ceramint

Effect of boron on phase, nanostructure, and thermal stability of polycarbosilane-derived SiC ceramics

Rahul Anand [a], Vempuluru Madhavi [a], Kathy Lu [a,b,*]

[a] *Department of Materials Science and Engineering, Virginia Tech, Blacksburg, VA, 24061, USA*
[b] *Department of Mechanical and Materials Engineering, University of Alabama at Birmingham, Birmingham, AL, 35294, USA*

ARTICLE INFO

Handling Editor: Dr P. Vincenzini

Keywords:
Boron
Silicon carbide
Phase
Microstructure
Thermal stability

ABSTRACT

The current study explores the formation, evolution, and thermal stability of polymer-derived SiBC at high temperatures. It focuses on the phase evolution of SiBC ceramics derived from the doping of boron in an allyl-containing polycarbosilane preceramic polymer after 1200 °C–1600 °C pyrolysis. Different SiBC ceramic monoliths have been obtained. Boron is incorporated into the carbon phase at lower pyrolysis temperatures but into both the carbon phase and the SiC lattice structure at high pyrolysis temperatures. B–C bonds form in SiBC and hinder the growth of graphitic carbon and SiC. Boron improves the densification and thermal stability of the SiBC ceramics. This work provides an improved understanding of boron effects in polymer-derived SiC nanostructures at high temperatures.

1. Introduction

Materials suitable for use in extreme conditions are attracting significant interest [1–4]. Polymer-derived SiCN, SiC, and SiBC are promising candidates with exceptional chemical, thermal, and mechanical stability [5]. The polymeric route also enables lower synthesis temperature and offers flexibility in tuning their microstructures, unlike conventionally produced borides, carbides, and nitrides [6]. Synthesis of silicon carbide (SiC) ceramics from various polymeric precursors, such as polycarbosilane, has been established [7–12]. Allylhydridopolycarbosilane (AHPCS) is a preferred polymer precursor in terms of processing versatility and obtaining stoichiometric SiC [13,14].

Doping different elements, such as boron, iron, lithium, calcium, chromium, zirconium, aluminum, and aluminum-yttrium, to SiC has been carried out to enhance or modify pressureless sintering of SiC [15–17]. Boron is one of the prominent dopants in enhancing densification and the corresponding thermal, mechanical, electrochemical, and electronic properties of SiC [6,13,18,19]. For polymer-derived SiC, the same benefit is observed. For example, SiC pyrolyzed from the AHPCS precursor was reported to have ~22.42 vol% porosity [14]. Precursor infiltration and pyrolysis (PIP) at 1700 °C after 4 cycles reduced porosity to ~7.87 vol%. In comparison, incorporation of 5 wt% borane dimethylsulfide to SiC reduced porosity to 4.27 vol% at 1700 °C without PIP cycles.

So far, there are few studies to understand the nanostructural changes due to boron-doping to polymer derived SiC [20,21]. A previous study suggests that boron doping to polymer-derived SiC does not lead to phase separation of boron containing crystalline phases such as B_4C [22]. Instead, incorporation of boron into polymer derived SiCN systems leads to exceptional increase in thermal, chemical, mechanical (creep) stabilities; oxidation resistance; and electronic properties [6]. Boron also enhances crystallization of polymer derived SiBCN systems by accelerating β-SiC phase formation while inhibiting Si_3N_4 phase nucleation [23,24]. This means that boron decreases the thermodynamic stability of SiBCN [25] and retards the carbothermal reduction of Si_3N_4 by forming turbostratic BC_xN layers [26]. Boron reduces the self-diffusion constant by retarding the mobility of N into the Si-B-N system, thus enhancing the thermal stability of Si_3N_4 [27]. In addition, boron incorporation into polymer derived SiOC reduces the amount of free carbon in the SiBOC ceramics by forming B–C bonds, which increases the complexity of the amorphous network by forming mixed boron oxycarbide units ($BO_{3\text{-}x}C_x$, $0 \le x \le 3$) [28,29]. Overall, the role of boron in the structural transformation of polymer derived ceramics at the nanostructural level is complex. The behavior of boron in the structural modification of precursor derived SiC needs to be explored.

In this work, a commercially available AHPCS precursor named SMP-10 was doped with 0–40 wt% BDMS and pyrolyzed from 1200 °C to 1600 °C. Microstructural and morphological evolution of SiC upon

---

[*] Corresponding author. Department of Materials Science and Engineering, Virginia Tech, Blacksburg, VA, 24061, USA.
E-mail address: klu@uab.edu (K. Lu).

https://doi.org/10.1016/j.ceramint.2024.10.222
Received 16 March 2024; Received in revised form 11 October 2024; Accepted 16 October 2024

modification with different concentrations of boron was investigated. The role of boron on the thermal stability of SiC at 2200 °C was evaluated.

2. Experimental procedure

2.1. Starting materials

For the preparation of SiC and boron-doped SiC monoliths, AHPCS (SMP-10, Starfire Systems, Inc., NY, USA) was employed as the SiC source, borane dimethylsulfide (BDMS, $BH_3·S(CH_3)_2$), Sigma Aldrich, USA) was used as the boron precursor. Toluene (Sigma Aldrich, USA) served as the solvent. A Karstedt's catalyst, platinum (0)-1,3-divinyl-1,1,3,3-tetramethyldisiloxane complex 2.1–2.4 wt% in xylene (Millipore Sigma, USA), was used as a crosslinking agent. An industrial grade Ar gas (99.99 % purity, AirGas, Christiansburg, VA, USA) was used throughout the synthesis process.

2.2. Sample preparation

Synthesis of boron-doped AHPCS specimens was conducted under controlled Ar conditions within a glove box. The preparation involved two solutions: solution 1 consisted of the AHPCS precursor dissolved in toluene (1:6 vol ratio); solution 2 was composed of the BDMS precursor dissolved in toluene (1:10 vol ratio). Solution 2 was carefully added dropwise to solution 1, and the resulting mixture was stirred for 15 min to ensure thorough mixing. The obtained single-source precursor was transferred into an aluminum pan and kept for 24 h for the reaction and solvent evaporation. After removing the solvent, the single-source precursor was dried at 80 °C in an argon atmosphere for 24 h. Argon was a protective atmosphere that allowed for possible crosslinking reactions and toluene solvent evaporation. Since the drying was done in the inert atmosphere of Ar, only toluene evaporation was involved. There were no reactions associated with the removal of the solvent as the boiling point of toluene is 110.6 °C. The dried and solidified precursor was punched out into discs of 14.5 diameter mm and crosslinked at 250 °C under a flowing Ar atmosphere.

The crosslinked polycarbosilane discs with boron-doping were pyrolyzed at 1200 °C, 1400 °C, and 1600 °C, respectively, for 2 h with a heating rate of 2 $°C·min^{-1}$ in a horizontal tubular furnace (CM Furnaces Inc., Bloomfield, NJ, USA) in a flowing Ar atmosphere. The cooling was carried out in flowing Ar at a 5 °C/min cooling rate. The flow of Ar was maintained as 5 ml s^{-1} throughout the process. Several sample batches were prepared using different weight ratios (5–40 wt%) of BDMS to SMP-10. For the synthesis of pure SiC, the AHPCS precursor was mixed with the Karstedt's catalyst (0.05 wt%) as a crosslinking initiator. After that, the AHPCS precursor was processed in the same way as described for the boron-doped AHPCS precursor.

2.3. Characterization

The polymer-to-ceramic conversion of the pure AHPCS and boron-doped AHPCS samples (after crosslinking at 80 °C) was investigated by thermogravimetric analysis (TGA, Model TGA 5500, TA Instruments, DE, USA) from room temperature to 1000 °C. The reason to carry out thermogravimetric analysis for the samples after crosslinking at 80 °C was to remove toluene so that the solvent effect was eliminated during the measurement. The toluene solvent was not part of the crosslinked polymer system and should not be included in understanding the pyrolysis process. FTIR spectra were recorded by a Fourier Transform Infrared Spectrophotometer (FTIR, Varian 670-IR, Varian Inc., USA). The phase evolution after pyrolysis was explored by scanning the SiC and SiBC specimens with an X-ray diffractometer (Wide Angle X-Ray Diffraction, XRD, Bruker D8, Bruker Nano GmbH, Berlin, Germany) using CuKα radiation (40 mA current, 40 kV accelerating voltage) from 20° to 80° with a step size of 0.03°.

Micro-Raman spectra were recorded with a confocal micro-Raman spectrometer (XploRA PLUS, Horiba Scientific, Piscataway, NJ, USA) equipped with a green laser (irradiation wavelength 532 nm) using a laser power source ranging from 1 to 2 μW.

To investigate the effect of boron on the morphology of the synthesized SiC monoliths at different pyrolysis temperatures, scanning electron microscopy (JSM IT-500HR, JEOL, Tokyo, Japan) was performed with a 20 kV accelerating voltage. X-ray photoelectron spectroscopy (XPS, PHI Quantera SXM-03, Kanagawa, Japan) was performed using an Al Kα X-ray (1486.7 eV) source. A low-energy electron beam (20 μA) was used to neutralize the charge on the surface, which allowed automatic charge compensation of the charged sample surfaces. The fractured surfaces of the samples were placed at an electron take-off angle of 55°. Multiple survey scans at different positions of the samples and the corresponding high-resolution peak scans were obtained after the ion milling. High resolution peaks were analyzed and fitted by PHI MultiPak software.

3. Results and discussion

3.1. Thermal changes

The FTIR spectra of the pure AHPCS and boron modified AHPCS precursors crosslinked at 250 °C are shown in Fig. 1. The pure AHPCS precursor sample shows peaks at wavenumbers of ~2915 cm^{-1} ($–CH_3$ stretching), ~2120 cm^{-1} (–Si–H stretching), ~1350 cm^{-1} ($-CH_3$ bending), ~1255 cm^{-1} ($Si–CH_3$ stretching), ~1034 cm^{-1} ($Si–CH_2–Si$ stretching), ~940 cm^{-1} (–Si–H deformation), ~820 cm^{-1} ($–Si–CH_3$ wagging), and ~733 cm^{-1} (Si–C stretching) [14,30]. The formation of $Si–CH_2–Si$ chain is mainly due to the hydrosilylation reaction between the monomers of AHPCS, an indication of polymerization. Further, the polymerization of AHPCS occurs as a result of dehydrocoupling reaction in which two Si–H groups combine and form Si-Si bonds. The peak intensities of stretching bond $–CH_3$ and $–CH_2–$ diminish for the boron-modified AHPCS precursor samples at all BDMS concentrations. In addition, the peak intensity of deformed –Si–H bonds decreases significantly. The stretched –Si–H peak intensity decreases gradually as the concentration of boron increases. This indicates the reaction between the borane group (BH_3) in the BDMS precursor and the allyl-containing monomers in the AHPCS precursor (hydroboration reaction). A vague allyl (C=C) stretching bond peak at 1680–1640 cm^{-1} is present in the pure AHPCS sample but is absent in the boron doped AHPCS samples. This indicates crosslinking in the BDMS-AHPCS precursor due to allyl group polymerization with borane [22]. Although B–C and Si–Si bonds are not identified in the FTIR spectra, the decrease of the Si–H bond intensity in the boron-doped AHPCS samples is believed to be caused by the same crosslinking process.

The ceramization of the crosslinked AHPCS and boron modified AHPCS samples with different concentrations of boron was studied by thermogravimetric (TG) analysis. A single step mass loss is observed for the pure AHPCS precursor sample (Fig. 2), which starts at ~300 °C and lasts until 950 °C. This mass loss can be attributed to the release of C_nH_m hydrocarbons and hydrogen [31,32]. The mass loss for the AHPCS sample is low compared to that reported elsewhere [14,30,31]. The decreased mass loss indicates better crosslinking of the AHPCS precursor. The total ceramic yield at 1000 °C is ~91.5 %. The BDMS containing AHPCS samples show single step mass loss curves similar to that of the pure AHPCS precursor, and the mass loss starts after 350 °C. The mass loss at 1000 °C for the sample containing 5 wt% BDMS (~5.2 wt%) is less compared to that of the pure AHPCS (~8.5 wt%). The increase in the ceramic yield (~94.8 %) is ascribed to the addition of boron containing group to the AHPCS monomers. For the AHPCS sample with 20 wt% BDMS, a negligible mass loss is observed. However, with further BDMS concentration increase, the ceramic yield of the BDMS-modified AHPCS sample decreases compared to that of the 5 wt% BDMS even though it is still higher than that of the pure AHPCS sample. The AHPCS sample with

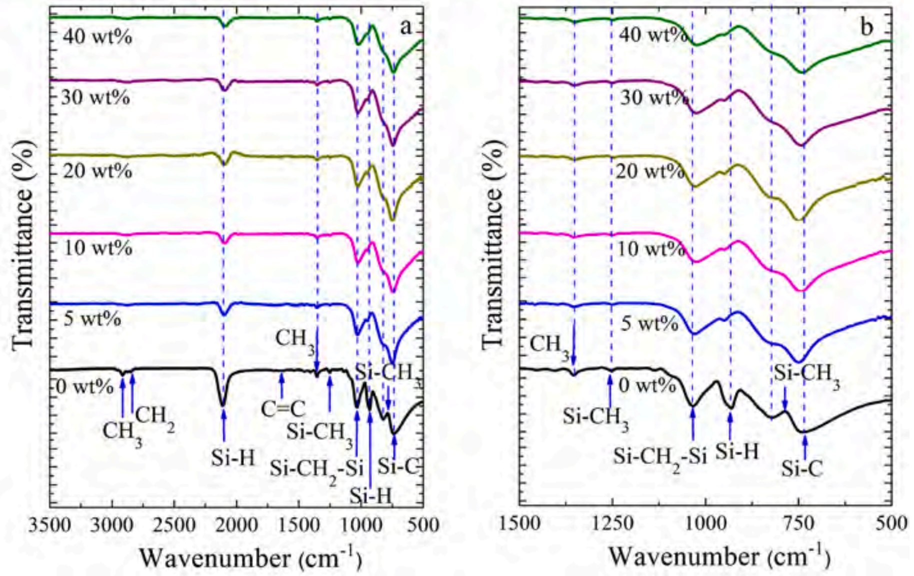

Fig. 1. FTIR spectra of BDMS (0–40 wt%)-doped AHPCS after crosslinking: a) overall spectra, b) enlarged spectra from 500 to 1500 cm^{-1}.

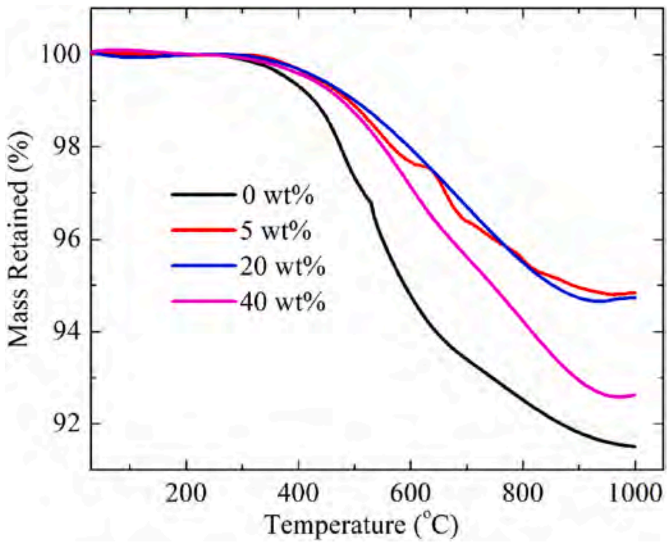

Fig. 2. Thermogravimetric curves of the crosslinked AHPCS and boron modified AHPCS samples.

40 wt% BDMS addition has a ceramic yield of 92.7 % at 1000 °C, which is lower than that of the 5 wt% BDMS (~94.8 %) and 20 wt% BDMS (~94.2 %) samples. Overall, the incorporation of BDMS increases the ceramic yield of AHPCS. We believe this is due to reduced volatilization of low-molecular-weight species, identified in the low temperature region during the AHPCS decomposition. The addition of BDMS accelerates the overall ceramization process.

3.2. Phase evolution

Fig. 3 shows the XRD patterns of the pure AHPCS and boron doped AHPCS pyrolyzed from 1200 to 1600 °C.

For the pure AHPCS pyrolyzed at 1200 °C, a vague graphitic carbon peak is observed at ~26.5°, revealing the (002) diffraction peak of graphitic carbon. The graphitic carbon peak intensity increases with increasing BDMS concentration up to 10 wt%. With further BDMS content increase, the graphitic carbon peak stays largely the same. β-SiC peaks are also present, indicating crystalline SiC formation, and the crystallinity gradually increases with the BDMS content, demonstrated by more defined SiC peaks, especially at 40 wt% BDMS.

For the samples pyrolyzed at 1400 °C and 1600 °C, an increase in the boron concentration above 5 wt% BDMS decreases the graphitic carbon peak intensity to an undetectable level (Fig. 3b and c), indicating that boron-doping to the AHPCS system makes the crystallization of the sp^2 carbon phase at high pyrolysis temperatures less significant as the boron atoms disrupt the regular arrangement of carbon atoms during pyrolysis. The β-SiC peaks sharpen with the increase of the pyrolysis temperature. A high concentration of boron (>5 wt% BDMS) seems to lead to narrower SiC peaks and accelerate the crystallization of SiC. However, the boron content effect on the SiC crystallization is less important than the pyrolysis temperature effect (Fig. 3b and c).

Shifts in the diffraction peak maxima for the β-SiC and sp^2 carbon phases are observed due to boron incorporation into the SiC matrix, which is illustrated in Fig. 4. At 1200 °C, the β-SiC peak indicates little or no right shift (Fig. 4a, diffused SiC peaks at 35.5°). At 1400 °C, however, the right shift of the β-SiC peaks for the boron-doped SiC (vs. pure SiC) is clear as given in the supplement (Fig. S1). At 1600 °C pyrolysis temperature, the β-SiC peaks for the boron-doped SiC again shift towards a higher Bragg's angle compared to that of the pure SiC sample (Fig. 4b), even though the fluctuation in the relative magnitude of shifts is not understood. The shifts indicate decreases in the β-SiC lattice spacing with increasing pyrolysis temperature, which we believe is primarily due to boron dissolution into the SiC lattice structure. Boron, being smaller in size than silicon, can lead to changes in the distances between neighboring atoms and introduce lattice distortions. In addition, boron introduces a hole (positive charge) due to the lower valence state compared to silicon. This charge compensation can lead to changes in the local environment of neighboring atoms and alter the lattice parameters. Such changes include bond lengths and angles within the SiC crystal lattice. Boron doping may also induce strain in the SiC crystal structure due to the size mismatch between boron and silicon, leading to local deformations in the lattice. The strain can affect the lattice parameters, causing shifts in X-ray diffraction peaks.

For the carbon phase, our observation is slightly different. At 1200 °C pyrolysis temperature, the graphitic carbon peaks are well-defined from the pure AHPCS pyrolyzed sample to the boron-doped AHPCS samples and shift to a higher diffraction angle (Fig. 4c), even though this effect diminishes at high BDMS concentrations again. This indicates boron incorporation into the carbon atomic structure, causing the lattice spacing to decrease. At 1600 °C pyrolysis temperature, the carbon

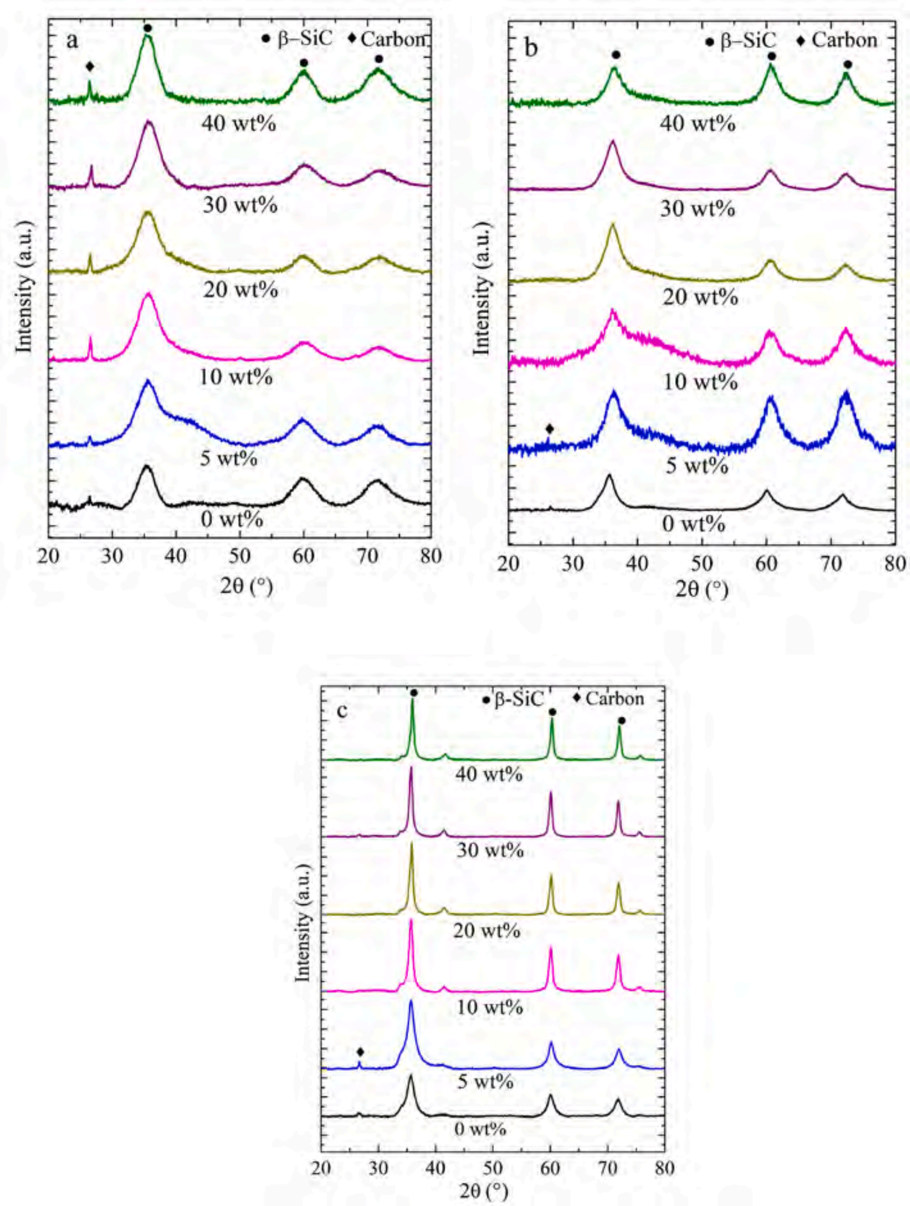

Fig. 3. XRD patterns of undoped and boron-doped AHPCS samples pyrolyzed at (a) 1200 °C, (b) 1400 °C, and (c) 1600 °C.

diffraction peaks still demonstrate the right shift even though some graphitic peaks are weak (Fig. 4d). This means that boron dissolves into the graphitic carbon even though this effect is overshadowed by other factors. At higher pyrolysis temperatures, boron incorporation into the lattice of graphitic carbon is less obvious but the incorporation into the β-SiC lattice is more observable, especially at higher BDMS concentrations. In general, boron diffusion into the graphitic carbon is more dominant at lower pyrolysis temperatures while the same is true for β-SiC at high pyrolysis temperatures. It should be noted that boron, even at 1600 °C, does not crystallize into a stable B_4C phase.

The effect of boron on the size of β-SiC crystallites is shown in Fig. 5. The crystallite size of β-SiC was calculated for all the samples following Scherrer's formula and using the maximum intensity peak at ~35.5° 2θ.

$$d = (0.89\ \lambda)\ /\ (\beta\ \mathrm{Cos}\ \theta) \tag{1}$$

d is the crystallite size, λ is the wavelength of the X-ray, β is the full width at half maximum of the most intense peak (in rad), and θ is half of the diffraction angle.

The crystallite size of β-SiC from the pure AHPCS is 3 nm, 3.2 nm, and 4.5 nm at pyrolysis temperatures of 1200 °C, 1400 °C, and 1600 °C, respectively. This increasing trend is as expected because higher pyrolysis temperatures cause more SiC crystallite growth. However, for the SiBC systems pyrolyzed at 1200 °C and 1400 °C, the crystallite size of β-SiC decreases with the BDMS concentration increase up to 10 wt%. For the SiBC ceramics pyrolyzed at 1600 °C, the crystallite size of β-SiC decreases from 4.5 to 4 nm when the BDMS dopant concentration changes from 0 to 5 wt%. At >5 wt% BDMS, the β-SiC crystal size increases again. This change occurs at a lower BDMS concentration than those at 1200 °C and 1400 °C pyrolysis temperatures. This result indicates that a small amount of boron hinders SiC crystallite growth; the same results were observed previously in the case of low concentration boron doping [21]. We believe boron inhibits carbon diffusion for SiC crystallite growth by dissolving into carbon atomic structures. However, a BDMS concentration of >10 wt% generally leads to increased β-SiC crystallite size, which increases rapidly with further boron content increase to 40 wt% BDMS (up to 11.7 nm). The same trend was reported in the case of polymer-derived boron-doped SiBOC system [28,29]. We conjecture that this is due to boron-induced fast diffusion in SiC, which

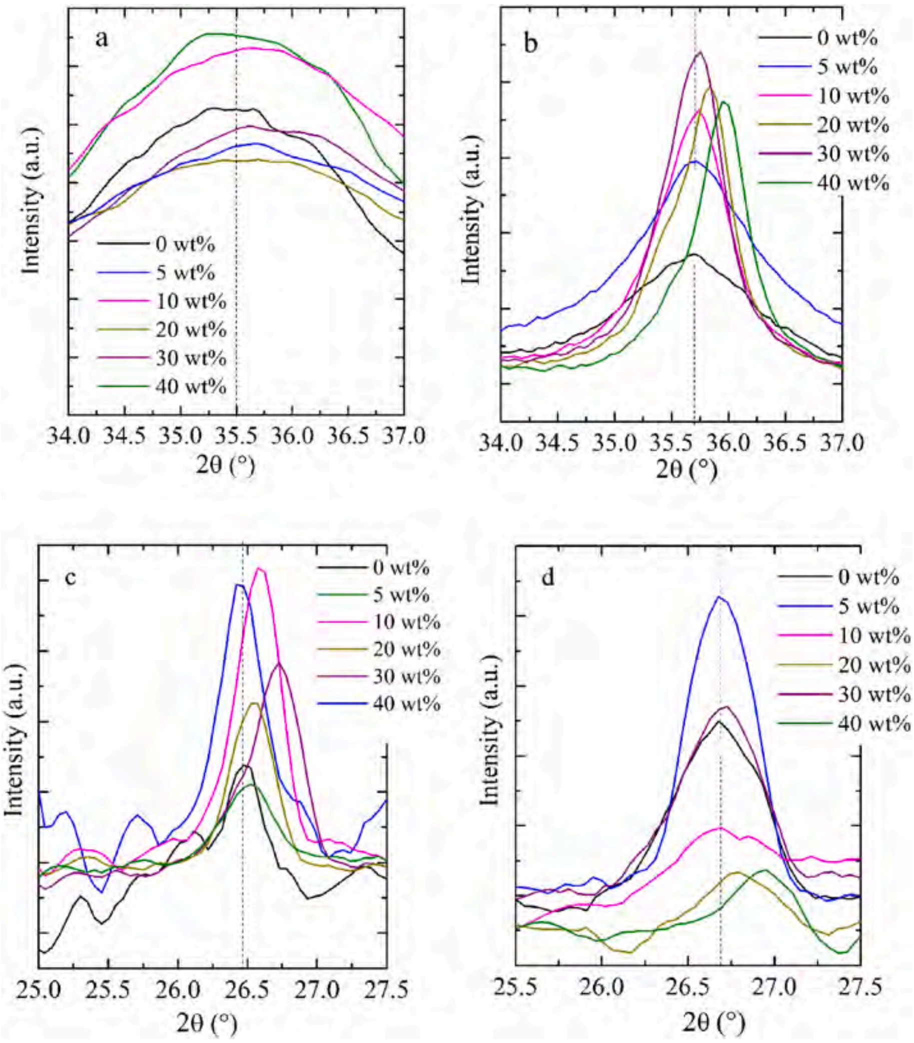

Fig. 4. SiC XRD peaks for the pure AHPCS and B-doped AHPCS pyrolyzed at (a) 1200 °C and (b) 1600 °C; graphitic carbon peaks for the corresponding samples pyrolyzed at (c) 1200 °C and (d) 1600 °C.

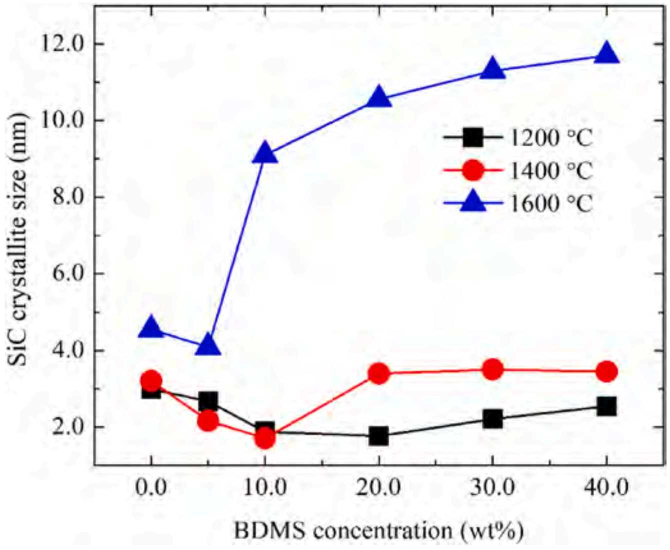

Fig. 5. Crystallite size of SiC at different boron concentrations and pyrolysis temperatures.

leads to the rapid growth of β-SiC crystals at 1600 °C. However, this boron-doping effect mainly happens at high pyrolysis temperatures, such as from 1400 to 1600 °C in Fig. 5. Some studies claim viscous flow promoted by the Si–B–C liquid phase formed at higher boron concentrations [33,34], which is yet to be confirmed. Also, the fast diffusion from boron doping at high pyrolysis temperatures for SiC growth is much higher than the steric hindrance effect from boron, thus leading to the SiC crystalline growth results in Fig. 5.

To understand the effect of boron incorporation into the carbon phase of the AHPCS-derived ceramics, the Raman spectra of the undoped and boron doped SiC pyrolyzed at 1200 °C and 1600 °C are shown in Fig. 6. As expected, the characteristic D peaks are observed near 1344 cm $^{-1}$; the characteristic G peaks are observed at ~1580 cm^{-1} and 1600 cm^{-1}, respectively, for all the specimens pyrolyzed at 1200 °C and 1600 °C.

At 1200 °C, the G peak, which is ascribed to sp^2 carbon, remains at the same wavenumber with a gradual increase in intensity and peak width as the BDMS content increases to 5 wt% and then to 30 wt% (Fig. 6). The G peak becomes less symmetrical and broadens toward higher wavenumbers, as the boron content is increased. This effect can be attributed to the broadening of the phonon spectra towards higher frequencies from the mixed bonds with boron, i.e., SiB_xC [35]. For the 1600 °C pyrolyzed samples, the broadening of the G peak for the 20 and 40 wt% BDMS samples indicates that boron doping does not facilitate

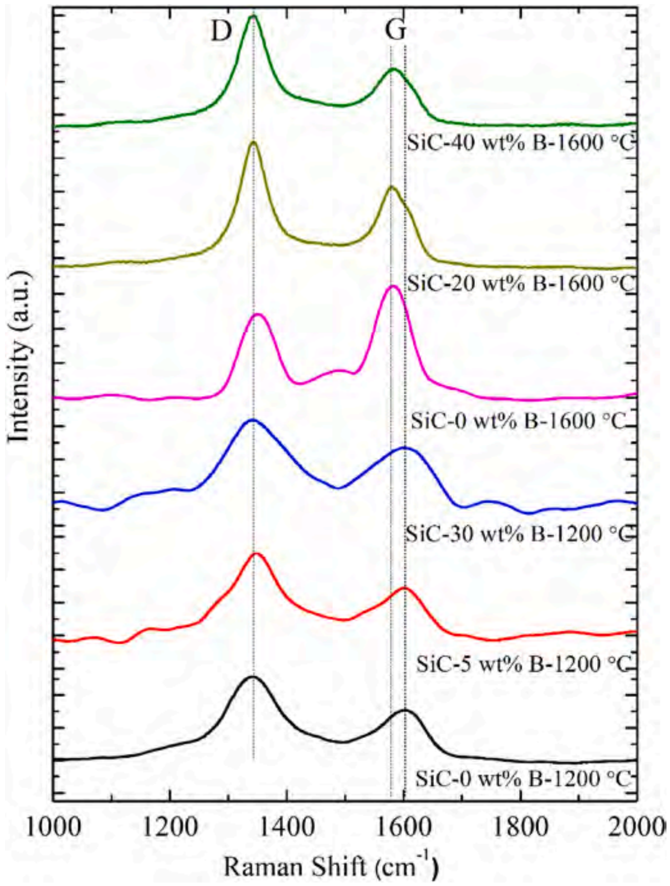

Fig. 6. Raman spectra of AHPCS and boron modified AHPCS pyrolyzed at 1200 °C and 1600 °C.

the crystallization of the graphitic carbon proportionally (Fig. 6). Also, the G peak has a left shift, again a sign of less graphitized carbon. Furthermore, the D peak becomes more intense for the 20 and 40 wt% BDMS samples, indicating increased carbon disorder, even at a much higher pyrolysis temperature of 1600 °C. Overall, boron doping to the SiC system increases the defective state. In conjunction with the XRD results (Figs. 3 and 4), this means that at relatively lower pyrolysis temperatures, boron doping to the SiC matrix increases the amorphous carbon more even though an increasing amount of graphitic carbon also forms. At higher pyrolysis temperatures, the total carbon amount is lower due to a more complete conversion to SiC ceramics, the graphitic carbon becomes undetectable. At the same time, the amorphous carbon phase becomes more defective, as shown in Fig. 6.

The graphitic carbon crystallite size (L_a) can be calculated using Eq. (2) [36]. C(λ) is assumed as ~4.95 nm at λ = 532 nm [37–41].

$$La = C(\lambda) \ / \ (I_{(D)} / \ I_{(G)}) \tag{2}$$

Table 1
Raman peak positions, peak intensity ratios, and carbon crystallite sizes in different pyrolyzed SiC and SiBC samples.

Samples	**Raman peak positions (cm $^{-1}$)**		$I_{(D)}$/ $I_{(G)}$	Carbon crystallite size (nm)
	D	G		(L_a)
0 wt% BDMS, 1200 °C	1346	1600	1.64	3.0
5 wt% BDMS, 1200 °C	1347	1595	1.93	2.6
30 wt% BDMS, 1200 °C	1346	1598	2.10	2.4
0 wt% BDMS, 1600 °C	1347	1581	0.67	7.4
20 wt% BDMS, 1600 °C	1344	1581	1.47	3.4
40 wt% BDMS, 1600 °C	1344	1580	1.72	2.9

As shown in Table 1, the L_a value of the boron-free samples is higher than that of the boron-containing samples. Boron doping to the SiC matrix reduces the size of the graphitic carbon clusters. This is the case for both low and high pyrolysis temperatures, which is also consistent with the XRD results in Fig. 3 that show stabilized graphitic peaks at 1200 °C with high BDMS contents and negligible graphitic peaks at 1600 °C with high BDMS contents. For the Raman spectra, higher intensity D peaks mean higher numbers of defects, and smaller clusters and rings (L_a) [22,42]. Doping boron creates defects in the carbon lattice and hinders graphitic carbon cluster growth. However, at lower pyrolysis temperatures, the boron doping effect cannot counter the effect of the large amount of graphitic carbon. Thus, graphitic carbon is detected through XRD (Fig. 3). However, the higher boron contents are able to keep the graphitic carbon peak at about the same intensity. At 1600 °C pyrolysis temperature, boron has an increased dissolution into SiC, which causes the SiC XRD peak to shift to the right (Fig. 3b) and SiC lattice spacing to decrease. Still, boron dissolves into carbon, the main effect is introducing a higher amount of disordered carbon.

To investigate the structural changes of boron-containing SiC, high-resolution XPS was performed on the pure and boron-containing SiC specimens pyrolyzed at 1600 °C. The deconvoluted XPS slow scan spectra of B 1s and C 1s (Fig. 7) reveal information about the nanostructure of the SiBC ceramics. The B1s peak at 190 eV and the C 1s peak at 281.7 eV indicate the formation of B–C bonds in the pyrolyzed SiBC ceramics, which is absent in the undoped SiC sample (Fig. 7a and b). This confirms the boron doping into the AHPCS-derived SiC matrix. Further, the peak intensity of the B–C bonds increases up to 20 wt% BDMS and becomes relatively stable above this concentration, indicating limited dissolution of boron into the carbon phase.

The other bonds are characterized as C–O (286.3 eV), C=C (284.5 eV), C–C (282.3 eV), and Si–C (280.1 eV) (Fig. 7b). The small amount of oxygen content in the SiBC (C-O bonds) is primarily due to the atmospheric exposure of the specimens after polymer casting and during transfer for cross-linking.

Fig. 7c shows the distributions of C–O, C–C (sp^2), C–C (sp^3), Si–C, and B–C bonds as a function of boron concentration in the SiBC ceramics. Each bond content was calculated by the ratio of deconvoluted areas of the corresponding C 1s peak. With the boron concentration increase, the amount of C–C (sp^3) bonds decreases and the amounts of Si–C and B–C bonds increase in the samples up to 20 wt% BDMS (Fig. 7c). Thus, boron consumes carbon in the SiBC matrix in the form of B–C bonds. The remaining free carbon is consumed in the form of new Si–C bonds. This is consistent with the understanding that boron is not conducive to the formation of graphitic carbon in the SiBC system. Above 20 wt% BDMS concentration, the samples show similar bond ratios. Thus, the maximum boron concentration that can be introduced into the SiC/C system is ~20 wt% BDMS, which is ~3.1 wt% boron (calculated based on the AHPCS ceramic yield) at 1600 °C. This boron solubility is higher than the maximum solubility of boron in graphite, i.e., ca. 2.35 wt% [43], which means that boron is incorporated into both carbon (graphitic carbon and amorphous carbon) and the SiC lattice structure, supported by the XRD and Raman results for the 1600 °C pyrolyzed samples.

3.3. *Atomic structure and morphological evolution*

The addition of boron also leads to changes in the atomic structure of the AHPCS-derived SiBC ceramics. The results for the SiC and SiBC ceramics pyrolyzed at 1600 °C are given in Fig. 8. The micrographs are also analyzed by inverse FFT (the images are provided in the supplement, Fig. S2). The inverse FFT image of the selected 'region 1' shows an interplanar distance of 0.379 nm, which corresponds to graphitic carbon in the SiC ceramic matrix [44]. For 'region 2', the inverse FFT-filtered image exhibits an interplanar distance of 0.251 nm, which corresponds to β-SiC [44]. This means the AHPCS-derived ceramics are C-excessive, consistent with the XRD results (Fig. 3). Some of the β-SiC

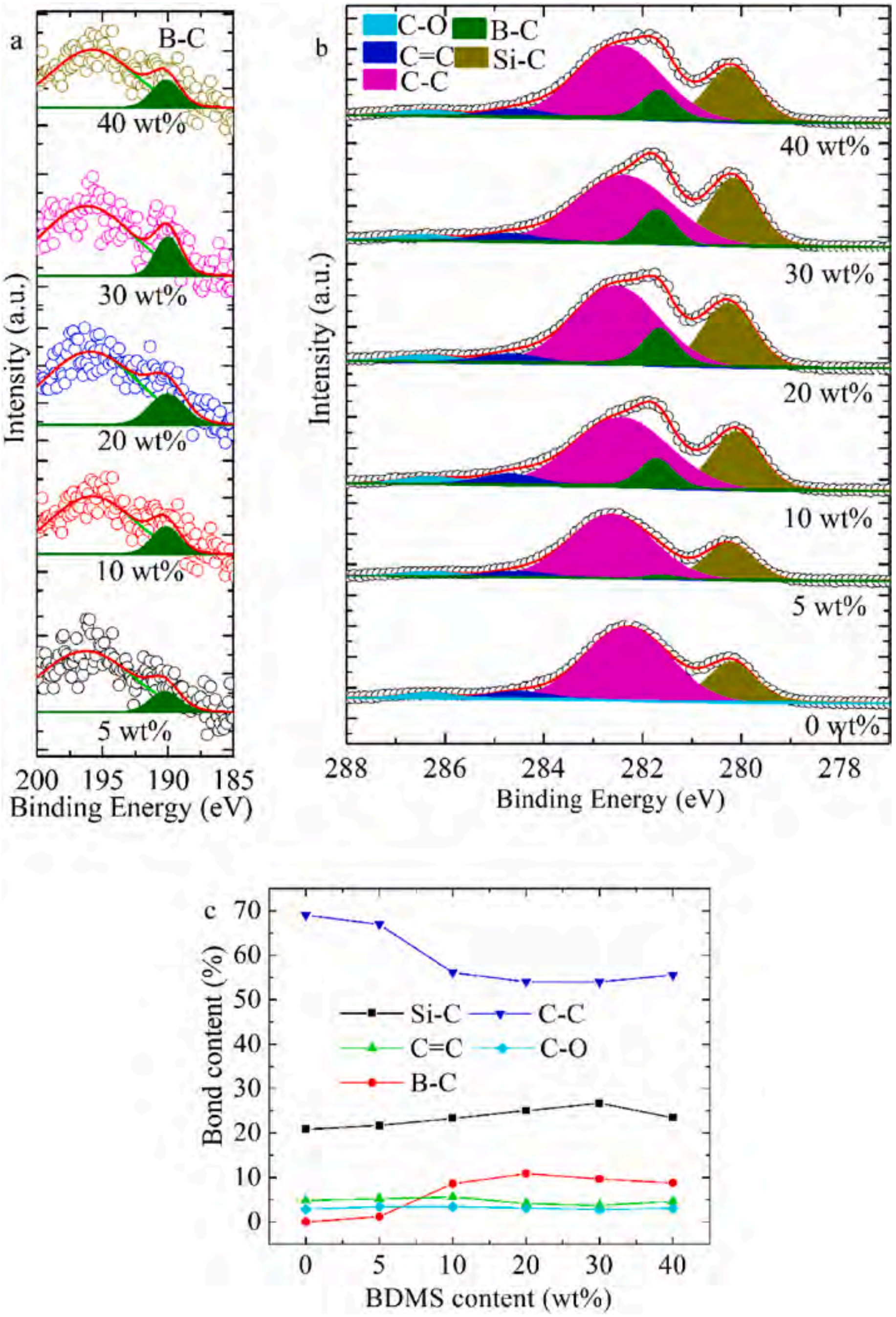

Fig. 7. XPS spectra of (a) B_{1s} and (b) C_{1s}, and (c) bond composition of SiBC for different BDMS content samples pyrolyzed at 1600 °C.

crystallites are adjacent and the graphitic carbon is located at the neck/junction area of these SiC crystallites. Only a few diffraction spots of graphitic carbon are observed. This is due to the low volume fraction of the graphitic carbon, and carbon remains mostly in the amorphous state.

In the case of boron-doped SiC (Fig. 8b and c), many crystal faults are visible. Different regions of 5 wt% BDMS doped SiBC (Fig. 8b, regions 3, 4, 5) were analyzed by inverse FFT. The d value in ‘region 4’ is 0.251 nm, corresponding to the β-SiC phase. However, d values of 0.371 nm and 0.359 nm are observed in ‘region 3’ and ‘region 5’, respectively. This lattice width corresponds to graphitic carbon. The slight decreases in the d values are due to the formation of the solid solution of boron and carbon (B_xC). This graphitic carbon is also observed in SiBC with 30 wt% BDMS (Fig. 8c). ‘Region 6’ shows lattice widths of 0.359 nm and 0.239 nm, which can be ascribed to the (111) plane of graphitic carbon and (200) plane of β-SiC crystals, respectively. The d value in ‘regions 7 and 10’ is calculated as 0.256 nm, which corresponds to the (111) plane of β-SiC crystals. Inverse FFT values in ‘region 8’ are 0.500 nm and 0.256 nm, which correspond to carbon (mostly in the form of carbon nanotubes) and β-SiC crystals, respectively. In ‘region 9’, the lattice width is 0.126 nm, corresponding to the (222) plane of β-SiC. This lattice spacing difference is due to the incorporation of boron into the SiC lattice. Regardless, no B_xC is identified. In some regions, such as ‘region 11 and region 12’, the lattices are distorted and short-ranged, promoted by the doping of boron into the SiC lattice [45]. These observations support the results obtained from the XRD (Figs. 3 and 4) and Raman analyses (Fig. 6). The FFT images of marked regions ‘10–12’ show lattice defects of β-SiC crystals due to the high concentration of boron in SiBC.

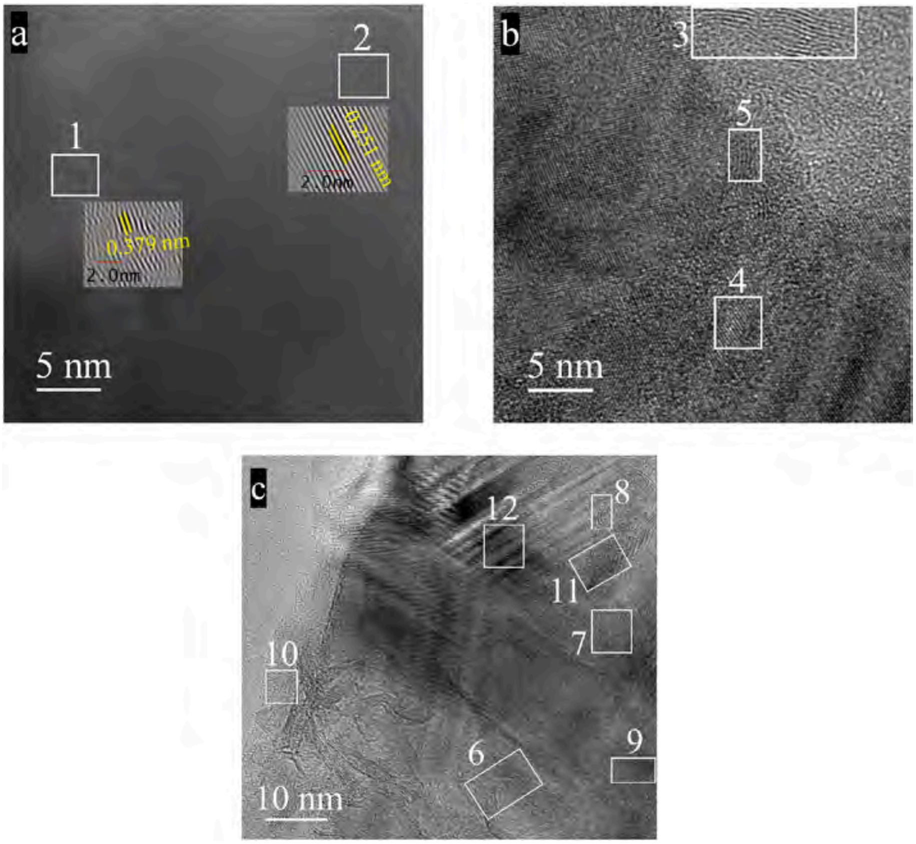

Fig. 8. TEM images showing features from (a) pure AHPCS, (b) AHPCS doped with 5 wt% BDMS, and (c) AHPCS doped with 30 wt% BDMS. All the samples were pyrolyzed at 1600 °C.

Fig. 9 shows that the pure SiC has a fully dense and defect-free microstructure at 1200 °C (Fig. 9a). With the pyrolysis temperature increase to 1400 °C (Fig. 9e), the microstructure still has an amorphous matrix, but some crystalline phases also form. A few pores are present. At 1600 °C pyrolysis temperature (Fig. 9i), the microstructure becomes mostly crystalline (the higher magnification image on the right); some small pores appear throughout the samples. For the boron-doped samples pyrolyzed at 1200 °C (Fig. 9b–d), the microstructure is amorphous, and no grains are observed at 1200 °C. The boron-doped SiC microstructures are mostly defect-free up to 20 wt% BDMS. At 40 wt% BDMS, a large pore is present. This means that the volatile species from the BDMS + AHPCS precursors are effectively removed through pyrolysis until this high BDMS content.

At 1400 °C pyrolysis temperature, boron doping causes the microstructure to change from an amorphous matrix to a crystalline structure (Fig. 9e–h). Boron addition promotes the crystallization of SiC, again consistent with the XRD results (Fig. 3). As the boron concentration increases, the SiC crystal size decreases. However, the pyrolyzed SiBC samples have pinhole defects of 1–3 μm at 1400 °C (Fig. 9f–h). Such defects are larger and more prominent at higher boron contents of 20 wt % and 40 wt% BDMS, as shown in Fig. 9g and h. These pores are believed to be from the removal of oxygen as CO/CO_2. The precursors used, allylhydridopolycarbosilane and borane dimethylsulfide, are highly reactive species. Even though the crosslinking was carried out in a controlled atmosphere glovebox, a trace amount of oxygen may be introduced. Also, during the transfer from the glovebox to the vacuum oven, the samples were briefly exposed to ambient air. Thus, we believe a very low amount of oxygen was present. Since excessive C is present in the pyrolyzed SiBC system, the following reactions occur to create the sparse pores observed: $2C + O_2 \rightarrow CO$ and $C + O_2 \rightarrow CO_2$.

At 1600 °C pyrolysis temperature, all the samples (from 0 to 40 wt% BDMS) have a crystalline structure. The size of the SiC crystallites increases compared to that at 1400 °C at the same boron concentration (Fig. 9j–l). The densification of the SiBC crystallites increases with the boron concentration at 1600 °C (Fig. 9i–l). The SiC crystal size has a minimal increase. The micropores/pinholes are few and the size gets smaller as the concentration of boron increases. Thus, the SiBC samples pyrolyzed at 1600 °C show few pores from 5 to 40 wt% BDMS concentrations (Fig. 9j–l). The 40 wt% BDMS sample has a dense microstructure except for one pore (Fig. 9l).

From the above observations, it can be stated that boron doping enhances the diffusion of silicon and carbon species, promoting the attachment and incorporation of these species into the SiC crystal lattice.

To investigate the effect of boron incorporation into SiC on microstructure stability at very high temperatures, the pure SiC samples and the samples with 5, 30, and 40 wt% BDMS (after pre-pyrolysis to remove all the evaporative species at 1000 °C) were annealed at 2200 °C for 1 h in an argon atmosphere. The pure SiC shows a continuously porous structure (Fig. 10a). In contrast, the boron-doped SiC (5 wt% BDMS) shows a denser structure (Fig. 10b). Increasing the boron content to 30 wt% BDMS leads to a fine crystalline, increasingly denser microstructure (Fig. 10c). Further increasing boron to 40 wt% BDMS shows complete densification of SiC (Fig. 10d). The porosity in the SiC at this high temperature is primarily due to the disintegration of Si-Si and Si-C bonds followed by sublimation of Si [44,46]. Thus, doping boron into the SiC structure enhances thermal stability by preventing the disintegration of Si-C bonds via the formation of a Si–B–C solid solution (Fig. 6).

As the boron concentration increases at 2200 °C, the SiC crystallite size decreases drastically. This suggests that boron can be incorporated into AHPCS-derived SiC to hinder the SiC grain growth and thus facilitate the densification of the SiBC specimens. At such a high temperature, we believe that boron and carbon form a low melting liquid phase B_xC and help to maintain the dense microstructure of the SiC monolith [33]. The addition of boron is also reported to accelerate the formation of

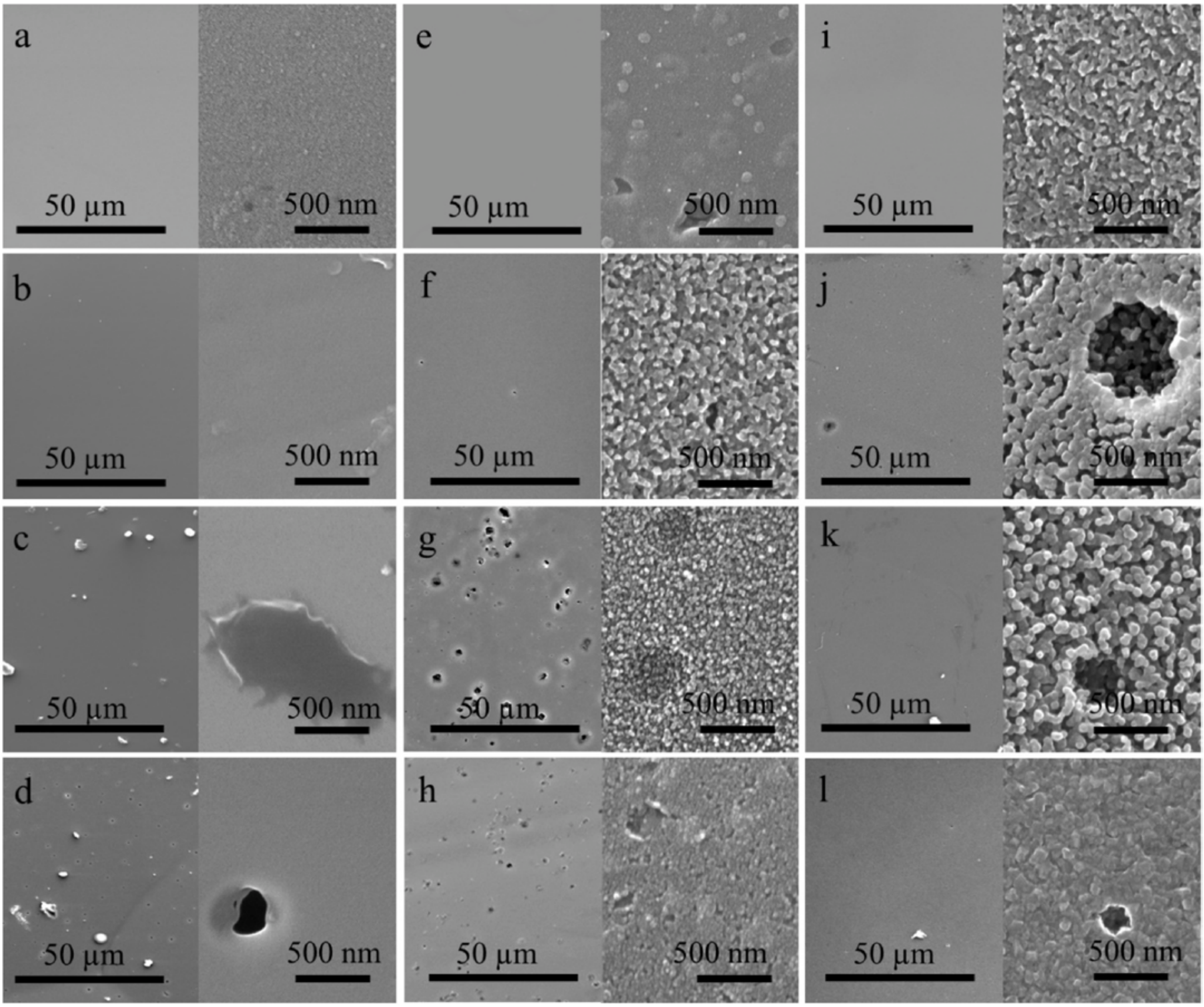

Fig. 9. Low (500x, left-hand side) and high (30000x, right-hand side) SEM micrographs of AHPCS modified with 0, 5, 20, and 40 wt% BDMS after different pyrolysis temperatures: (a–d) 1200 °C, (e–h) 1400 °C, and (i–l) 1600 °C.

point defects, improving the densification kinetics of SiC ceramics [47]. A solid solution of boron in SiC lowers the activation energy for self-diffusion through the SiC lattice and hence enhances densification [48,49]. This observation is consistent with the XRD results in Fig. 5.

4. Conclusions

The present work explores the influence of boron doping on the microstructure and thermal stability of polymer-derived SiC ceramics. Incorporation of boron into AHPCS improves the SiBC ceramic yield to as high as ~94 % after 1000 °C pyrolysis. Boron interacts with carbon in the SiC matrix and forms B–C bonds. The crystallite size of graphitic carbon decreases continuously with an increase in the boron concentration. The introduction of 5 wt% BDMS to AHPCS reduces SiC crystallite size during pyrolysis. However, higher concentrations of boron in SiC accelerate SiC crystal growth, especially at a high pyrolysis temperature of 1600 °C. Boron is incorporated into the lattice of graphitic carbon at lower pyrolysis temperatures (<1400 °C) but also diffuses into the β-SiC lattice at higher pyrolysis temperatures. Defect-free and dense microstructures of SiBC are obtained for the samples pyrolyzed at 1200 °C with up to 20 wt% BDMS. At 1600 °C and 40 wt% BDMS, the SiBC microstructure is also almost fully dense. The B_xC/SiB_xC solid solution improves the microstructural stability of boron-doped SiC at 2200 °C.

CRediT authorship contribution statement

Rahul Anand: Writing – original draft, Visualization, Validation, Investigation, Formal analysis, Data curation. **Vempuluru Madhavi:** Investigation, Data curation. **Kathy Lu:** Writing – review & editing, Visualization, Validation, Supervision, Software, Resources, Project administration, Methodology, Funding acquisition, Formal analysis, Conceptualization.

Funding information

This work received financial support from the National Science Foundation under Grant No. CBET-2024546and the Air Force Office of Scientific Research under grant number FA9550-22-1-0081.

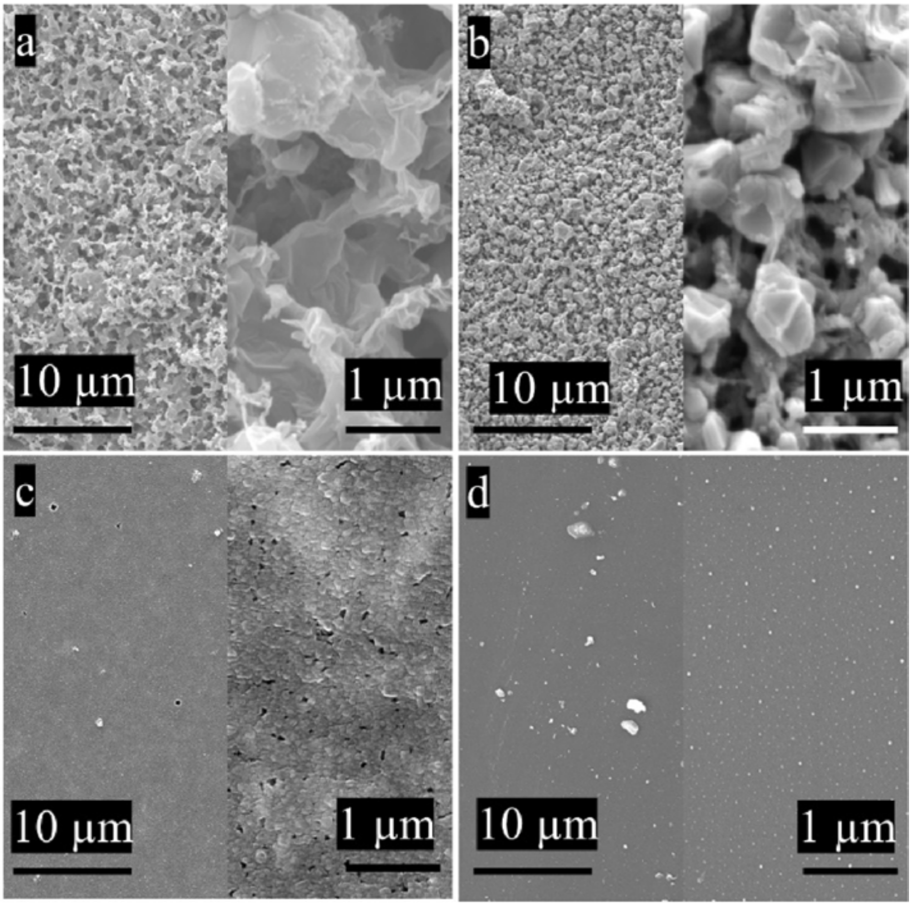

Fig. 10. Low (1000x, left-hand side) and high (30,000x, right-hand side) magnification SEM micrographs of SiBC modified with (a) 0 wt%, (b) 5 wt%, (c) 30 wt%, and (d) 40 wt% BDMS after treatment at 2200 °C for 1 h.

Declaration of competing interest

The authors declare the following financial interests/personal relationships which may be considered as potential competing interests:

Kathy Lu reports financial support was provided by National Science Foundation. Kathy Lu reports financial support was provided by Air Force Office of Scientific Research.

Acknowledgment

The authors would like to acknowledge the financial support from National Science Foundation and Air Force Office of Scientific Research.

Appendix A. Supplementary data

Supplementary data to this article can be found online at https://doi.org/10.1016/j.ceramint.2024.10.222.

References

[1] N.P. Padture, Advanced structural ceramics in aerospace propulsion, Nat. Mater. 15 (8) (2016) 804–809.
[2] R. Naslain, Design, preparation and properties of non-oxide CMCs for application in engines and nuclear reactors: an overview, Compos. Sci. Technol. 64 (2) (2004) 155–170.
[3] D.R. Clarke, M. Oechsner, N.P. Padture, Thermal-barrier coatings for more efficient gas-turbine engines, MRS Bull. 37 (10) (2012) 891–898.
[4] S. Packirisamy, K.J. Sreejith, D. Devapal, B. Swaminathan, Polymer-derived ceramics and their space applications, in: Y. Mahajan, J. Roy (Eds.), Handbook of Advanced Ceramics and Composites: Defense, Security, Aerospace and Energy Applications, Springer International Publishing, Cham, 2020, pp. 1–107.
[5] E. Ionescu, S. Bernard, R. Lucas, P. Kroll, S. Ushakov, A. Navrotsky, R. Riedel, Polymer-derived ultra-high temperature ceramics (UHTCs) and related materials, Adv. Eng. Mater. 21 (8) (2019) 1900269.
[6] P. Colombo, G. Mera, R. Riedel, G.D. Sorarù, Polymer-derived ceramics: 40 years of research and innovation in advanced ceramics, J. Am. Ceram. Soc. 93 (7) (2010) 1805–1837.
[7] A.B. Shelekhin, E.J. Grosgogeat, S.-T. Hwang, Gas separation properties of a new polymer/inorganic composite membrane, J. Membr. Sci. 66 (2) (1992) 129–141.
[8] S. Yajima, Y. Hasegawa, J. Hayashi, M. Iimura, Synthesis of continuous silicon carbide fibre with high tensile strength and high Young's modulus, J. Mater. Sci. 13 (12) (1978) 2569–2576.
[9] M.J. Wild, P. Buhler, On the phase composition of polymethylsiloxane derived ceramics, J. Mater. Sci. 33 (22) (1998) 5441–5444.
[10] X. Bao, M.J. Edirisinghe, G.F. Fernando, M.J. Folkes, Precursors for silicon carbide synthesised from dichloromethylsilane derivatives, J. Eur. Ceram. Soc. 18 (7) (1998) 915–922.
[11] D. Pizon, L. Charpentier, R. Lucas, S. Foucaud, A. Maître, M. Balat-Pichelin, Oxidation behavior of spark plasma sintered ZrC–SiC composites obtained from the polymer-derived ceramics route, Ceram. Int. 40 (3) (2014) 5025–5031.
[12] M.F. Gozzi, M.d.C. Gonĉalves, I.V.P. Yoshida, Near-stoichiometric silicon carbide from a poly(methylsilylene)/tetra-allylsilane mixture, J. Mater. Sci. 34 (1) (1999) 155–159.
[13] S.C. Zunjarrao, A. Rahman, R.P. Singh, Characterization of the evolution and properties of silicon carbide derived from a preceramic polymer precursor, J. Am. Ceram. Soc. 96 (6) (2013) 1869–1876.
[14] S. Kaur, R. Riedel, E. Ionescu, Pressureless fabrication of dense monolithic SiC ceramics from a polycarbosilane, J. Eur. Ceram. Soc. 34 (15) (2014) 3571–3578.
[15] M. Omori, H. Takei, Pressureless sintering of SiC, J. Am. Ceram. Soc. 65 (6) (1982) c92, c92.
[16] E.R. Maddrell, Pressureless sintering of silicon carbide, J. Mater. Sci. Lett. 6 (4) (1987) 486–488.
[17] R.A. Alliegro, L.B. Coffin, J.R. Tinklepaugh, Pressure-sintered silicon carbide, J. Am. Ceram. Soc. 39 (11) (1956) 386–389.
[18] K. Uchiyama, T. Yamamoto, Y. Einaga, Fabrication and electrochemical properties of boron-doped SiC, Carbon 174 (2021) 240–247.
[19] A. Viard, D. Fonblanc, D. Lopez-Ferber, M. Schmidt, A. Lale, C. Durif, M. Balestrat, F. Rossignol, M. Weinmann, R. Riedel, S. Bernard, Polymer derived Si–B–C–N ceramics: 30 years of research, Adv. Eng. Mater. 20 (10) (2018) 1800360.

[20] A.R. Puerta, E.E. Remsen, M.G. Bradley, W. Sherwood, L.G. Sneddon, Synthesis and ceramic conversion reactions of 9-BBN-modified allylhydridopolycarbosilane: a new single-source precursor to boron-modified silicon carbide, Chem. Mater. 15 (2) (2003) 478–485.

[21] Z. Yu, Y. Fang, M. Huang, R. Li, J. Zhan, C. Zhou, G. He, H. Xia, Preparation of a liquid boron-modified polycarbosilane and its ceramic conversion to dense SiC ceramics, Polym. Adv. Technol. 22 (12) (2011) 2409–2414.

[22] S. Kaur, G. Mera, R. Riedel, E. Ionescu, Effect of boron incorporation on the phase composition and high-temperature behavior of polymer-derived silicon carbide, J. Eur. Ceram. Soc. 36 (4) (2016) 967–977.

[23] H. Schmidt, W. Gruber, G. Borchardt, P. Gerstel, A. Müller, N. Bunjes, Coarsening of nano-crystalline SiC in amorphous Si–B–C–N, J. Eur. Ceram. Soc. 25 (2) (2005) 227–231.

[24] A.H. Tavakoli, P. Gerstel, J.A. Golczewski, J. Bill, Effect of boron on the crystallization of amorphous Si–(B–)C–N polymer-derived ceramics, J. Non-Cryst. Solids 355 (48) (2009) 2381–2389.

[25] A.H. Tavakoli, J.A. Golczewski, J. Bill, A. Navrotsky, Effect of boron on the thermodynamic stability of amorphous polymer-derived Si(B)CN ceramics, Acta Mater. 60 (11) (2012) 4514–4522.

[26] A. Jalowiecki, J. Bill, F. Aldinger, J. Mayer, Interface characterization of nanosized B-doped Si_3N_4/SiC ceramics, Compos. Appl. Sci. Manuf. 27 (9) (1996) 717–721.

[27] K. Matsunaga, Y. Iwamoto, Molecular Dynamics study of atomic structure and diffusion behavior in amorphous silicon nitride containing boron, J. Am. Ceram. Soc. 84 (10) (2001) 2213–2219.

[28] R. Peña-Alonso, G. Mariotto, C. Gervais, F. Babonneau, G.D. Soraru, New insights on the high-temperature nanostructure evolution of SiOC and B-doped SiBOC polymer-derived glasses, Chem. Mater. 19 (23) (2007) 5694–5702.

[29] M.A. Schiavon, C. Gervais, F. Babonneau, G.D. Soraru, Crystallization behavior of novel silicon boron oxycarbide glasses, J. Am. Ceram. Soc. 87 (2) (2004) 203–208.

[30] B. Santhosh, E. Ionescu, F. Andreolli, M. Biesuz, A. Reitz, B. Albert, G.D. Sorarù, Effect of pyrolysis temperature on the microstructure and thermal conductivity of polymer-derived monolithic and porous SiC ceramics, J. Eur. Ceram. Soc. 41 (2) (2021) 1151–1162.

[31] Z. Yu, M. Huang, Y. Fang, R. Li, J. Zhan, B. Zeng, G. He, H. Xia, L. Zhang, Modification of a liquid polycarbosilane with 9-BBN as a high-ceramic-yield precursor for SiC, React. Funct. Polym. 70 (6) (2010) 334–339.

[32] I.L. Rushkin, Q. Shen, S.E. Lehman, L.V. Interrante, Modification of a hyperbranched hydridopolycarbosilane as a route to new polycarbosilanes, Macromolecules 30 (11) (1997) 3141–3146.

[33] L. Stobierski, A. Gubernat, Sintering of silicon carbide II. Effect of boron, Ceram. Int. 29 (4) (2003) 355–361.

[34] J. Wan, M.J. Gasch, A.K. Mukherjee, In situ densification behavior in the pyrolysis consolidation of amorphous Si-N-C bulk ceramics from polymer precursors, J. Am. Ceram. Soc. 84 (10) (2001) 2165–2169.

[35] K. Terauds, R. Raj, Limits to the stability of the amorphous nature of polymer-derived HfSiCNO compounds, J. Am. Ceram. Soc. 96 (7) (2013) 2117–2123.

[36] L.G. Cançado, K. Takai, T. Enoki, M. Endo, Y.A. Kim, H. Mizusaki, A. Jorio, L. N. Coelho, R. Magalhães-Paniago, M.A. Pimenta, General equation for the determination of the crystallite size La of nanographite by Raman spectroscopy, Appl. Phys. Lett. 88 (16) (2006) 163106.

[37] A.C. Ferrari, J. Robertson, Interpretation of Raman spectra of disordered and amorphous carbon, Phys. Rev. B 61 (20) (2000) 14095–14107.

[38] D.S. Knight, W.B. White, Characterization of diamond films by Raman spectroscopy, J. Mater. Res. 4 (2) (2011) 385–393.

[39] M.J. Matthews, M.A. Pimenta, G. Dresselhaus, M.S. Dresselhaus, M. Endo, Origin of dispersive effects of the Raman D band in carbon materials, Phys. Rev. B 59 (10) (1999) R6585–R6588.

[40] F. Tuinstra, J.L. Koenig, Raman spectrum of graphite, J. Chem. Phys. 53 (3) (1970) 1126–1130.

[41] T. Jiang, Y. Wang, Y. Wang, N. Orlovskaya, L. An, Quantitative Raman analysis of free carbon in polymer-derived ceramics, J. Am. Ceram. Soc. 92 (10) (2009) 2455–2458.

[42] C. Liu, K. Li, H. Li, S. Zhang, Y. Zhang, X. Hou, Synthesis, characterization, and ceramization of a SiC–ZrC–C preceramic polymer precursor, J. Mater. Sci. 50 (7) (2015) 2824–2831.

[43] C.E. Lowell, Solid solution of boron in graphite, J. Am. Ceram. Soc. 50 (3) (1967) 142–144.

[44] R. Anand, K. Lu, Fate of polymer derived SiC monolith at different high temperatures, J. Anal. Appl. Pyrol. 178 (2024) 106386.

[45] T. Wang, Y. Zhang, P. Karandikar, C. Ni, Structural evolution in reaction-bonded silicon carbide and boron carbide composites (RBSBC), Ceram. Int. 44 (2) (2018) 2593–2598.

[46] Y. Zhang, T. Chen, J. Chen, Q. Zhang, Y. Gou, The effects of annealing atmosphere and intrinsic component on high temperature evolution behaviors of SiC fibers, Mater. Sci. Eng. 848 (2022) 143363.

[47] M.S. Datta, A.K. Bandyopadhyay, B. Chaudhuri, Sintering of nano crystalline α silicon carbide by doping with boron carbide, Bull. Mater. Sci. 25 (3) (2002) 181–189.

[48] S. Prochazka, R.M. Scanlan, Effect of boron and carbon on sintering of SiC, J. Am. Ceram. Soc. 58 (1–2) (1975) 72, 72.

[49] R. Malik, Y.-W. Kim, Effects of initial α-phase content on properties of pressureless solid-state sintered SiC ceramics, Int. J. Appl. Ceram. Technol. 19 (2) (2022) 703–712.